

# Investigation of Nonlinear Optical (NLO) Response of Metal Complexes via Quantitative Structure-Activity Relationship (QSAR) Method

Fazira Ilyana Abdul Razak<sup>a,b,c,\*</sup>, Suhaila Sapari<sup>d</sup>, Yee Shi Wee<sup>a</sup>, Lee Yang Ning<sup>a</sup>

<sup>a</sup> Department of Chemistry, Faculty of Science, Universiti Teknologi Malaysia, 81310 UTM Johor Bahru, Johor, Malaysia.

<sup>b</sup> Centre for Sustainable Nanomaterials, Universiti Teknologi Malaysia, 81310 UTM Johor Bahru, Johor, Malaysia.

<sup>c</sup> Department of Physics, Faculty of Science and Technology, Universitas Airlangga, 60115 Surabaya, Indonesia

<sup>d</sup> School of Chemical and Energy Engineering, University Technology Malaysia, 81310, UTM, Johor Bahru, Johor, Malaysia.

## Article history

Received

16 August 2025

Revised

30 October 2025

Accepted

30 October 2025

Published online

31 November 2025

\*Corresponding author  
faziraillyana@utm.my

## Abstract

Quantitative structure–activity relationship (QSAR) models establish a quantitative link between the chemical structure of compounds and their activity, providing insight into how specific fragments or sub-structures influence properties. Nonlinear optics (NLO) studies phenomena arising from changes in a material's optical characteristics under light, where interactions can produce new optical fields with altered phase, frequency, amplitude, polarization, or propagation path. Experimental development of NLO materials is often costly and time-consuming, requiring multiple procedural steps. Computational approaches, such as QSAR, can more efficiently predict the NLO potential of compounds, reducing the need for extensive experimentation. In this study, nine metal complexes were geometrically optimized using Gaussian 16 and analyzed using QSAR. Structure 4 was the most stable, with the lowest optimization energy of  $-0.7132$  a.u., while Structure 6 had the lowest HOMO–LUMO energy gap of  $0.16354$  eV. Structure 2 exhibited the highest dipole moment ( $11.85$  D), and Structure 5 showed the lowest ( $0.00$  D). QSAR analysis revealed that the HOMO–LUMO energy gap contributed most significantly to the NLO response of these metal complexes, with an  $R^2$  value of  $0.445$ . These results highlight the potential of computational QSAR as an effective tool for predicting NLO behaviour in metal complexes. Further research is necessary to improve prediction accuracy and to deepen understanding of structure–property relationships in NLO materials.

**Keywords** Quantitative structure–activity relationship (QSAR), nonlinear optics (NLO), metal complexes

© 2025 Penerbit UTM Press. All rights reserved

## 1.0 INTRODUCTION

Nonlinear optics (NLO) is a branch of optical science that investigates phenomena arising when the response of a material to light becomes nonlinear, leading to the generation of new optical fields with altered phase, frequency, amplitude, polarization,

or propagation characteristics (Stucky, 1991). Unlike linear optical processes, NLO effects depend nonlinearly on the intensity of the incident electromagnetic field, making them highly sensitive to molecular and electronic structure. The advent of lasers in 1960 provided the high-intensity, coherent light necessary to observe these effects, catalyzing a surge of interest in the development and application of NLO materials (Maiman, 1960). Recent advances in rational structure design and computational modelling have further accelerated the discovery of high-performance NLO materials, offering deeper insight into structure–property relationships (Yan et al., 2024; Biaggio, 2024; Wang et al., 2024). NLO materials have become integral to numerous technological domains, including photonic communications, optical data storage, signal processing, medical imaging, and sensing devices, as they enable the manipulation and transmission of information via photons rather than electrons (Hagar, 2016). Despite their potential, the experimental discovery and optimization of high-performance NLO materials remain resource-intensive, requiring multiple iterative steps to assess stability, optical response, and functional performance.

NLO-active compounds can generally be classified as organic, inorganic, or hybrid materials. Organic compounds, particularly azobenzenes, have received considerable attention due to their tunable structural and electronic properties, rapid response times, and strong optical nonlinearity. Azobenzenes exhibit  $\pi \rightarrow \pi^*$  electronic transitions that dominate their visible absorption spectra, and their optical behaviour is highly sensitive to the nature and position of substituents (Buttingsrud, 2007). Such properties have facilitated applications as dyes and active components in photonic systems, including optical data storage and switching (Eich, 1987; Wiesner, 1990; Natansohn, 1992). More recently, studies on low-dimensional organic nanomaterials and molecular crystals have demonstrated enhanced NLO responses due to strong charge-transfer interactions and tunable band structures (Biaggio, 2024; Wang et al., 2024). In contrast, inorganic materials—including metal oxides, chalcogenides, and coordination complexes—offer superior thermal and chemical stability, while metal complexes provide the flexibility to fine-tune NLO properties by modifying the metal center, ligands, or coordination geometry. Emerging classes such as nitrides and halide-based frameworks have also demonstrated promising NLO efficiencies through controlled electronic polarization and structural anisotropy (Yan et al., 2024). Hybrid organic–inorganic systems aim to combine the advantages of both classes but remain underexplored due to challenges in synthesis and characterization.

Quantitative structure–activity relationship (QSAR) modelling has emerged as a powerful computational tool for predicting the physical, chemical, and optical properties of compounds based on their molecular structures (Hansch, 1991; Cronin, 2009). QSAR relies on molecular descriptors, geometric, electronic, topological, and physicochemical, to capture the essential features that influence a target property (Popelier, 1999; Dudek, 2006). Advanced descriptor frameworks, such as Bader's atoms-in-molecules (AIM) theory, provide detailed insights into electronic topology, bridging quantum mechanical calculations and classical chemical bonding concepts (Alsberg, 2000; O'Brien, 2001). Recent computational studies have integrated density functional theory (DFT) descriptors with machine-learning algorithms to enhance QSAR predictive accuracy for complex NLO systems (Wang et al., 2024). Statistical and chemometric methods, including partial least squares (PLS) regression and variable selection, allow researchers to identify influential descriptors and address multicollinearity, thereby improving predictive accuracy for nonlinear properties (Wold, 1983; Thompson, 1978). QSAR has been successfully applied to azobenzene dyes, where descriptors such as bond length, electron density, and frontier molecular orbital energies have been correlated with  $\pi \rightarrow \pi^*$  transition energies, providing predictive insight into optical behaviour (Astrand, 2000; Astrand, 2001; Buttingsrud, 2007).

Despite its utility, the application of QSAR to NLO materials remains limited, particularly for metal complexes. Previous studies have mainly focused on organic chromophores, evaluating parameters such as thermal stability, solubility, and second-order NLO coefficients, while often neglecting detailed electronic descriptors or metal-based systems (Berhanu, 2012; Luan, 2012; Karelson, 2000). Metal complexes represent promising NLO candidates due to their tunable electronic structures, polarizability, and coordination environments, which strongly influence band gap, dipole moment, and hyperpolarizability. However, systematic investigations linking these features to NLO responses are scarce. Addressing this gap is crucial for the rational design of efficient NLO materials and for enabling predictive computational screening to reduce experimental cost and time.

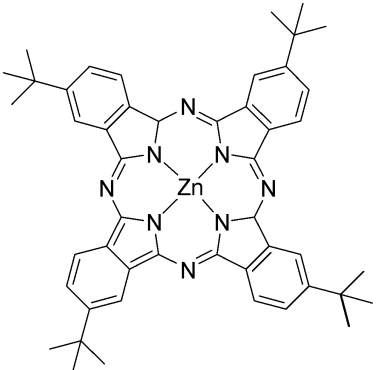
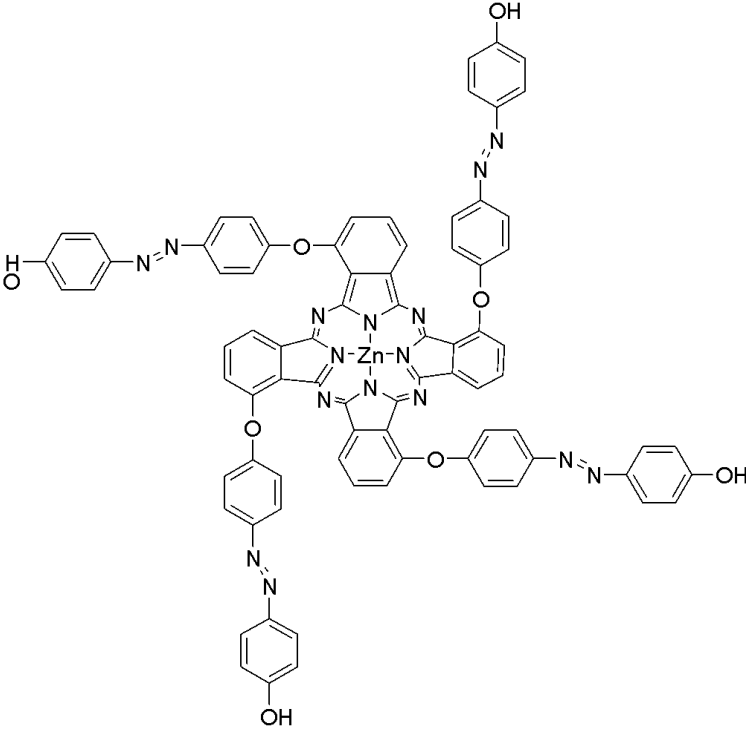
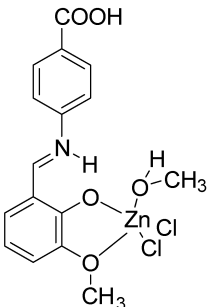
The present study aims to develop a QSAR-based computational framework for predicting NLO properties in metal complexes. By combining quantum chemical calculations with Gaussian16 and molecular descriptor analysis—including HOMO–LUMO energy gap, dipole moment, and electronic structure parameters—this work seeks to identify the structural and electronic factors that most significantly influence NLO responses. This approach provides a systematic methodology for predicting NLO behaviour, facilitating the design of efficient materials with potential applications in photonics, optoelectronics, and data storage. By extending QSAR methodology to metal-based NLO systems, this study addresses a critical research gap. It provides a computational framework to guide experimental development and accelerate the discovery of next-generation NLO materials.

## 2.0 EXPERIMENTAL

### 2.1 Structure Identification

The experimental values for all the structures are obtained from previous works by various researchers. Table 1 below shows all the structures used for this study.

**Table 1:** Structure Identification

No.	Structure	Reference
1.		Kumar et al., 2007
2.		Chen et al., 2011
3.		Kamaal et al., 2021

4.

Thilak et al., 2013
  
5.

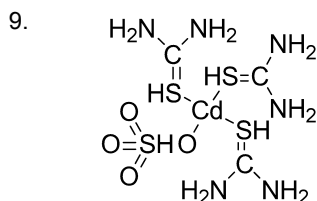
$$\text{S}=\text{Nb}=\text{S}$$

Maldonado et al., 2020
  
6.

Chen et al., 2011
  
7.

Chen et al., 2011
  
8.

Dhanuskodi et al., 2011



Dhanuskodi et al.,  
2011

## 2.2 Experimental NLO

Experimental NLO properties, specifically the nonlinear refractive index ( $n_2$ ), were obtained from previous studies summarized in Table 1. In these studies, the Z-scan technique was employed with wavelengths in the 600–800 nm range. Optical limiting measurements were conducted by simultaneously recording incidents and transmitted pulse energies using the same Z-scan setup, ensuring accurate determination of the NLO response.

## 2.3 Geometry Optimization and Electronic Structure Calculation

All molecular structures were constructed using *GaussView 6.0* and optimized using the semi-empirical PM6 method (Buttingsrud et al., 2007) as implemented in *Gaussian 16*. The PM6 method was selected for its balance between computational efficiency and accuracy, particularly for large systems and transition-metal complexes (Stewart, 2007; Najim et al., 2022). All geometry optimizations were carried out in the gas phase at 298 K, using the default *Gaussian* convergence criteria.

Following optimization, the total electronic energy of each structure was recorded, and key electronic parameters—including the highest occupied molecular orbital (HOMO), lowest unoccupied molecular orbital (LUMO), HOMO–LUMO energy gap, dipole moment, and total electronic energy—were extracted for QSAR analysis. The same computational approach was subsequently applied to calculate the second-order hyperpolarizability ( $\beta_{\text{tot}}$ ) using the keyword “polar=gamma” to incorporate polarization effects within the PM6 framework.

The optimized geometries of all nine molecules were validated to ensure the reliability of the computational results. Frequency analyses were performed at the PM6 level to verify that all optimized structures correspond to true minimum on the potential energy surface, as indicated by the absence of imaginary frequencies. Additionally, key structural parameters, including selected bond lengths and bond angles, were compared with experimental X-ray crystallographic data available in the literature (Chen et al., 2011; Buttingsrud et al., 2007; Najim et al., 2022). The optimized geometries showed consistent trends and acceptable deviations relative to the experimental data, confirming the suitability of the PM6 method for these molecular systems.

## 2.4 QSAR Modelling and Descriptor Analysis

QSAR modelling was performed in Discovery Studio using the “Calculate Molecular Properties” module on a workstation equipped with an Intel Core i7 processor. Dmol<sup>3</sup> calculations were carried out using the B3LYP functional. Molecular descriptors derived from Gaussian16 outputs were used as input variables to construct predictive QSAR models. Multiple Linear Regression (MLR) was applied to correlate molecular descriptors with NLO properties, generating both regression equations and graphical representations. These models allowed the identification of key structural and electronic features that influence NLO behaviour, thereby achieving the primary objective of this study.

### 2.4.1 Data Input

The descriptors used in this study were selected based on their relevance to NLO performance. Conjugation was represented by the number of double bonds in each molecule, and the effect of metal incorporation was quantified using metal mass. Table 2 summarizes the values for all descriptors across the nine studied structures.

**Table 2:** Values of Descriptors

Structure	Number of Double Bonds	Metal Mass (g/mol)
1	17	65.38
2	47	65.38
3	7	65.38
4	4	182.19
5	2	92.91
6	33	63.55
7	33	58.69
8	6	65.38
9	6	112.41

3.0 RESULTS AND DISCUSSION

3.1 Experimental NLO Data (Z-Scan)

The nonlinear refractive index ( $n_2$ ) values were obtained from previous studies using the Z-scan technique, with measurement wavelengths ranging from 600 to 800 nm. Table 3 summarizes the experimentally reported  $n_2$  values for the nine structures. These data serve as reference values to compare with the calculated NLO parameters.

Table 3: Experimental Results

Structure	$n_2$ Value (cm <sup>2</sup> /W)	Reference
1	$1.14 \times 10^{-15}$	Kumar et al., 2007
2	$3.30 \times 10^{-16}$	Chen et al., 2011
3	$-1.35 \times 10^{-7}$	Kamaal et al., 2021
4	$9.41 \times 10^{-8}$	Thilak et al., 2013
5	$3.00 \times 10^{-16}$	Maldonado et al., 2020
6	$3.70 \times 10^{-16}$	Chen et al., 2011
7	$3.40 \times 10^{-16}$	Chen et al., 2011
8	$-5.22 \times 10^{-8}$	Dhanuskodi et al., 2011
9	$-7.71 \times 10^{-8}$	Dhanuskodi et al., 2011

3.2. Geometry Optimization and Electronic Structure Data

The molecular structures were constructed in GaussView 6.0 and optimized in Gaussian 16 using the Semi-Empirical Method (PM6), which balances computational efficiency and accuracy, particularly for large systems (Stewart, 2007). The optimized structures were analyzed for key electronic properties, including the Highest Occupied Molecular Orbital (HOMO), Lowest Unoccupied Molecular Orbital (LUMO), HOMO–LUMO energy gap, dipole moment, and second-order hyperpolarizability ( $\beta_{tot}$ ). From Table 4, among the nine structures studied, Structure 7 exhibited the highest optimization energy (1.0288 a.u.). In contrast, Structure 4 had the lowest (-0.7133 a.u.), consistent with trends reported in similar PM6 studies where larger molecules typically show higher optimization energies (Baba et al., 2012). In addition, structure 7, with the highest optimization energy, is due to the bulky substituents, which induce steric hindrance and a non-planar geometry, thereby limiting  $\pi$ – $\pi$  conjugation and reducing molecular stability. Conversely, Structure 4 showed the lowest optimization energy due to its planar and well-conjugated framework, which facilitates effective electron delocalization and enhances overall structural stability. Structure 2 displayed the highest dipole moment (11.85 D), whereas Structure 5 had a zero-dipole moment, reflecting the symmetrical nature of the molecule, as observed in previous reports (Buttingsrud et al., 2007). For HOMO and LUMO energies, Structure 4 had the highest HOMO (-11.8465 eV), and Structure 5 had the lowest LUMO (-3.4093 eV), yielding a HOMO–LUMO energy gap ranging from 0.1635 eV (Structure 6) to 8.1180 eV (Structure 4), which agrees with earlier PM6-based calculations for similar systems (Najim et al., 2022).

Table 4: Geometry Optimization and Electronic Structure Results

Structure	Optimization Energy (a. u.)	Dipole Moment (D)	HOMO (eV)	LUMO (eV)	HOMO–LUMO energy gap (eV)
1	0.2366	6.42	-7.6162	-6.3879	1.2283
2	0.5048	11.85	-7.5792	-6.3922	1.1870
3	-0.3751	6.04	-8.3955	-6.1005	2.2950
4	-0.7133	10.33	-11.8465	-3.7285	8.1180
5	0.1963	0.00	-7.5430	-3.4093	4.1337
6	0.7382	5.96	-5.4940	-5.3304	0.1635
7	1.0288	9.45	-7.4143	-6.3027	1.1116
8	-0.2963	3.07	-6.1138	-3.8161	2.2977
9	-0.2140	7.59	-5.5114	-3.7097	1.8017

Following the analysis of electronic properties, the second-order hyperpolarizability ( $\beta_{tot}$ ) values were obtained from Gaussian16 calculations using the Semi-Empirical Method (PM6) with the “polar=gamma” keyword to account for polarization effects (Liyanage et al., 2003). The  $\beta_{tot}$  was calculated as  $\beta_{tot} = \sqrt{(x^2 + y^2 + z^2)}$ , where x, y, and z components were extracted from the Gaussian log files. From Table 5, structure 2 exhibited the highest  $\beta_{tot}$  ( $2305.1450 \times 10^{-30}$  esu). In contrast, Structure 5 could not be calculated because it has a zero-dipole moment, highlighting the necessity of a non-zero dipole for reliable hyperpolarizability calculations (Buttingsrud et al., 2007).

Table 5: Second Order Hyperpolarizability,  $\beta_{tot}$  Values

Structure	$\beta_{tot}$ ( $\times 10^{-30}$ esu)
1	2290.0896
2	2305.1450
3	464.0151
4	9.7953
5	-
6	1699.3825
7	521.6618
8	29.1029
9	39.5433

When comparing structures with the same metal, such as Structures 1, 2, 3, and 8 (all Zn-based), the  $\beta_{tot}$  increases with the number of aromatic rings, consistent with reports that extended  $\pi$ -conjugation enhances nonlinear optical (NLO) responses (Kamal et al., 2019; Musafia & Senderowitz, 2010). For structures sharing the same framework but differing in metal mass, such as Structures 6 vs. 7 and 8 vs. 9, higher metal mass corresponds to increased  $\beta_{tot}$ , demonstrating the contribution of the metal center to NLO activity (Peterson et al., 2009). Comparison of Structures 6, 7, 8, and 9 also indicates that lower HOMO–LUMO energy gap generally correlates with higher  $\beta_{tot}$  values, supporting trends linking smaller HOMO–LUMO gaps to enhanced hyperpolarizabilities (Karelsen, 2000; Shim & MacKerell, 2011).

When the calculated  $\beta_{tot}$  values are compared with the experimental nonlinear refractive index ( $n_2$ ) values obtained from Z-scan measurements, a positive correlation is observed, despite some differences arising from solvent effects in the experiments and gas-phase calculations in Gaussian16. For instance, Structure 6, which has the lowest HOMO–LUMO energy gap (0.1635 eV), exhibits the third-highest  $\beta_{tot}$  but shows a higher  $n_2$  value than Structure 2, indicating that lower HOMO–LUMO energy gap structures generally produce stronger NLO responses experimentally. Similarly, trends in metal mass and conjugation also correspond to experimental  $n_2$  trends, confirming the predictive value of the computational approach while highlighting the influence of experimental conditions on absolute NLO magnitudes (Berhanu et al., 2012; Luan et al., 2012). Overall, the combined analysis of computational and experimental data demonstrates that  $\beta_{tot}$  is strongly influenced by conjugation, metal identity, dipole moment, and electronic structure, providing valuable guidance for the design of high-performance NLO materials.

3.3 QSAR Study

In this study, all geometrically optimized compounds were used for QSAR calculations to investigate the relationship between molecular descriptors and nonlinear optical (NLO) response. The calculations involved four descriptors, each considered individually: HOMO–LUMO energy gap, metal mass, dipole moment, and conjugation. QSAR models were developed using

Multiple Linear Regression (MLR), which allows correlation of each descriptor with the NLO response, providing predictive insights for the design of future NLO materials.

The QSAR analysis generated linear plots correlating each descriptor with the NLO response ( $\beta_{\text{tot}}$ ). Figure 1 shows the relationship between HOMO–LUMO energy gap and NLO response, indicating a positive trend where lower HOMO–LUMO energy gap energies correspond to higher  $\beta_{\text{tot}}$  values. Figure 2 shows the correlation between metal mass and NLO response, indicating that heavier metals generally enhance  $\beta_{\text{tot}}$ . Figures 3 and 4 display the effects of dipole moment and conjugation, respectively, both of which showed weaker correlations than HOMO–LUMO energy gap and metal mass.

The goodness-of-fit for each descriptor was evaluated using  $R^2$  values, as summarized in Table 6. HOMO–LUMO energy gap exhibited the strongest correlation with NLO response ( $R^2 = 0.445$ ), followed by metal mass ( $R^2 = 0.308$ ), while dipole moment ( $R^2 = 0.118$ ) and conjugation ( $R^2 = 0.002$ ) had comparatively minor effects. Although the  $R^2$  values are below 0.5, they are still considered acceptable for preliminary QSAR analyses, particularly when dealing with small, structurally diverse datasets. Moderate  $R^2$  values can still provide valuable qualitative insights into descriptor–property relationships rather than predictive accuracy (Roy et al., 2016; Chirico & Gramatica, 2012).

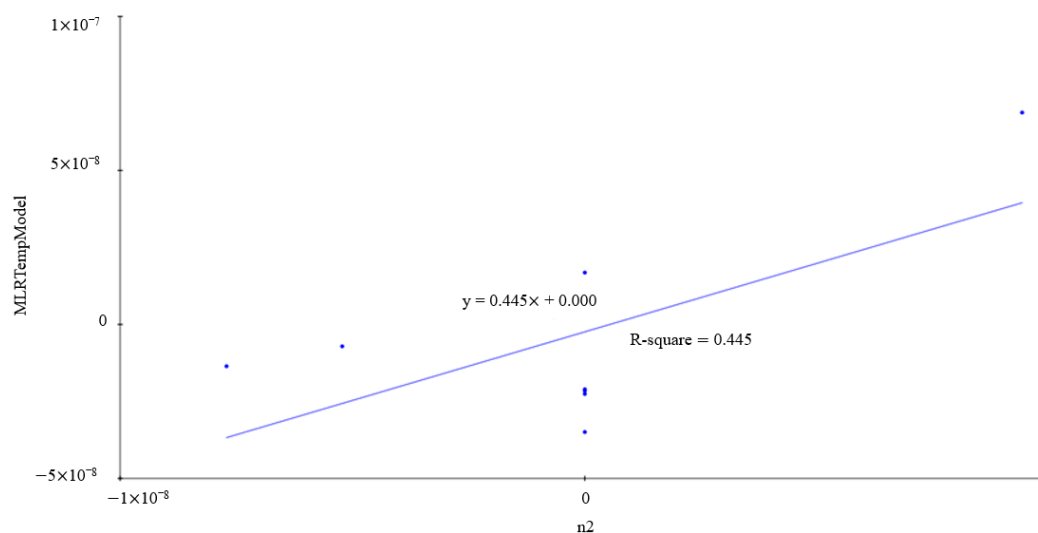


**Figure 1:** QSAR Analysis Plot on HOMO–LUMO energy gap

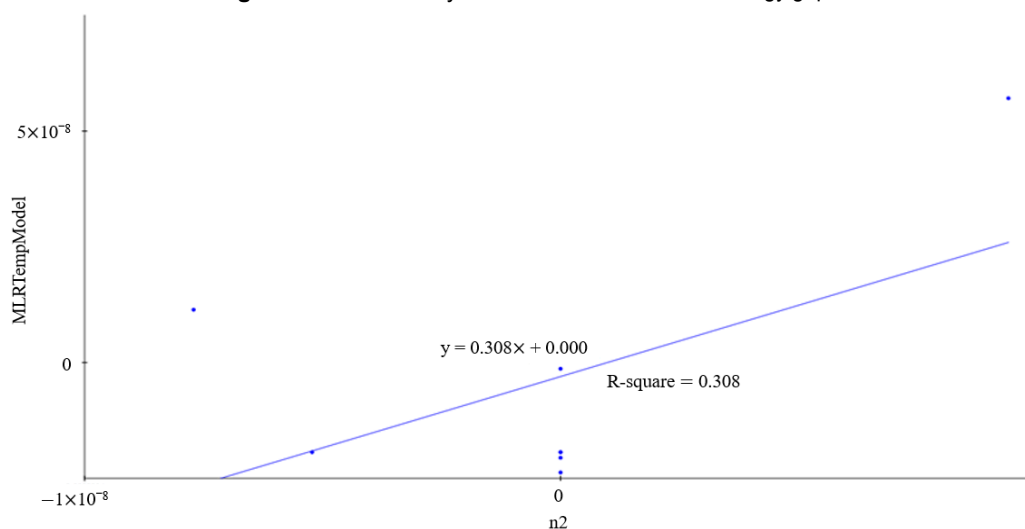


**Figure 2:** QSAR Analysis Plot on Metal Mass



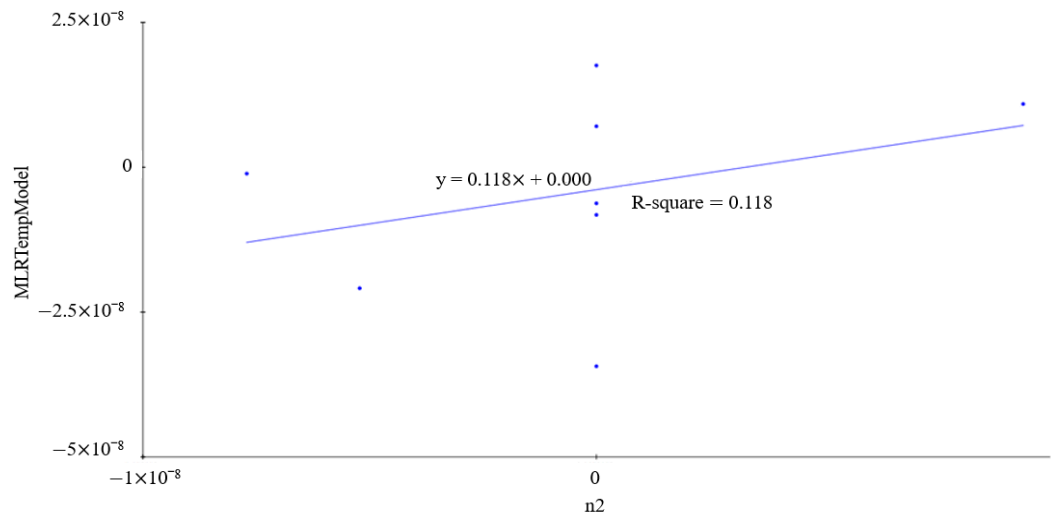


Figure 3: QSAR Analysis Plot on Dipole Moment

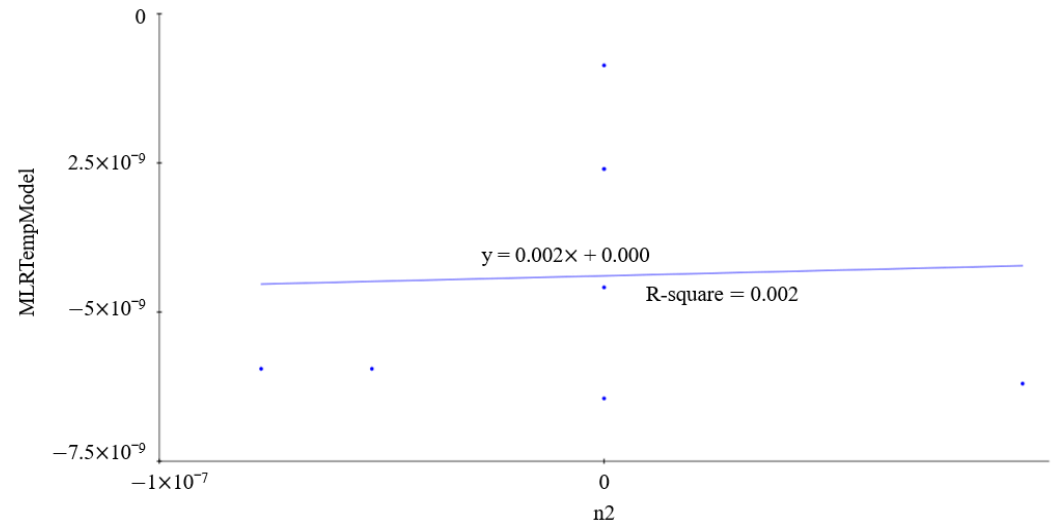


Figure 4: QSAR Analysis Plot on Conjugation

Table 6: R<sup>2</sup> Values

Effect	R <sup>2</sup>	Equation
HOMO–LUMO energy gap	0.445	y = 0.445x
Metal Mass	0.308	y = 0.308x
Dipole Moment	0.118	y = 0.118x
Conjugation	0.002	y = 0.002x

Following the identification of key descriptors, the NLO performance of individual structures was examined using  $\beta_{\text{tot}}$  values in combination with descriptor data. Table 7 presents the relationship between  $\beta_{\text{tot}}$ , experimental  $n_2$  values, HOMO–LUMO energy gap, and metal mass for all nine structures. It can be observed that the calculated  $\beta_{\text{tot}}$  generally follows the trend of the experimental  $n_2$  values, despite variations arising from differences between gas-phase calculations and solvent-phase experimental measurements. For example, Structure 6, which had the lowest HOMO–LUMO energy gap (0.1635 eV), exhibited the third highest  $\beta_{\text{tot}}$  ( $1699.3825 \times 10^{-30}$  esu), while Structure 2 had the highest  $\beta_{\text{tot}}$  ( $2305.1450 \times 10^{-30}$  esu) even though its HOMO–LUMO energy gap was higher. This suggests that although a lower HOMO–LUMO energy gap typically enhances NLO response, other factors, such as the molecular environment and structural arrangement, also influence  $\beta_{\text{tot}}$ . Similarly, the effect of metal mass on NLO response is highlighted by comparisons between Structures 6 and 7 and Structures 8 and 9, in which heavier metals correlate with higher  $\beta_{\text{tot}}$  values.

Table 7: NLO Relationship

Structure	$\beta_{\text{tot}}$ ( $\times 10^{-30}$ esu)	$n_2$ Value ( $\text{cm}^2/\text{W}$ )	HOMO–LUMO energy gap (eV)	Metal Mass (g/mol)
1	2290.0896	$1.14 \times 10^{-15}$	1.2283	65.38
2	2305.1450	$3.30 \times 10^{-16}$	1.1870	65.38
3	464.0151	$-1.35 \times 10^{-7}$	2.2950	65.38
4	9.7953	$9.41 \times 10^{-8}$	8.1180	182.19
5	-	$3.00 \times 10^{-16}$	4.1337	92.91
6	1699.3825	$3.70 \times 10^{-16}$	0.1635	63.55
7	521.6618	$3.40 \times 10^{-16}$	1.1116	58.69
8	29.1029	$-5.22 \times 10^{-8}$	2.2977	65.38
9	39.5433	$-7.71 \times 10^{-8}$	1.8017	112.41

These results demonstrate that QSAR models can successfully predict trends in NLO properties based on individual molecular descriptors. However, in this study, QSAR calculations were limited to one descriptor at a time due to the insufficient number of metal complexes with available  $n_2$  values. Nevertheless, this preliminary analysis provides a valuable framework for future studies, in which multi-descriptor models can be constructed using larger datasets to enhance predictive accuracy and guide the design of high-performance NLO materials.

These QSAR analyses also provided practical insights for the design of new NLO materials. By inserting the metal mass and HOMO–LUMO energy gap values into the developed models, one can estimate whether a target compound will exhibit a favourable NLO response without extensive experimental testing, thereby facilitating the screening of potential candidates (Kamal et al., 2019; Peterson et al., 2009). While this study was limited to single-descriptor correlations due to the limited number of metal-containing compounds with available  $n_2$  values, it establishes a foundation for future multi-parameter QSAR investigations, in which the combined effects of conjugation, metal type, dipole moment, and HOMO–LUMO energy gap could be systematically evaluated to enhance predictive accuracy.

Overall, the QSAR results confirm that HOMO–LUMO energy gap and metal mass are the dominant contributors to NLO behaviour, while dipole moment and conjugation play secondary roles. These findings align with theoretical predictions and previous experimental observations, providing a reliable framework for rational design of high-performance NLO chromophores in future studies (Liyanage et al., 2003; Buttingsrud et al., 2007).

## 4.0 CONCLUSION

In this study, the computational and QSAR analyses revealed that among the factors investigated, HOMO–LUMO energy gap is the dominant contributor to the NLO response of the studied metal complexes, followed by metal mass. Structures with lower HOMO–LUMO energy gap, such as Structure 6, exhibited higher second-order hyperpolarizability ( $\beta_{\text{tot}}$ ), confirming that a smaller HOMO–LUMO energy gap facilitates electron excitation and enhances polarizability, leading to more substantial NLO effects. Metal mass also plays a secondary role, with heavier metals often increasing NLO responses through enhanced charge-transfer interactions. Dipole-moment and conjugation showed relatively minor influence in the present dataset. These findings indicate that future studies should prioritize tuning the HOMO–LUMO energy gap through molecular design and careful metal selection to optimize NLO performance. Expanding the dataset with additional geometrically optimized structures and experimental  $n_2$  values and employing higher-accuracy methods for metal-containing complexes would enable more robust QSAR models and more precise predictions. Overall, this work demonstrates a promising strategy for guiding the rational design of high-performance NLO materials, highlighting band gap engineering as a key pathway for next-generation photonic applications.

## Acknowledgement

This project was funded by the Ministry of Higher Education, Malaysia, for the Fundamental Research Grant Scheme FRGS 5F471 (FRGS/1/2021/STG04/UTM/02/7) and Universiti Teknologi Malaysia UTM CG, PY/2024/02436/Q.J130000.3054.05M08). The author would also like to thank the Faculty of Science, Universiti Teknologi Malaysia and Computing Information Center Technology for providing a High-Performance Computer for the Gaussian 16 simulation.

## References

- [1] Alsberg, B. K., Popelier, P. L. A., & O'Brien, J. P. (2000). Topological analysis of electron density in molecular systems. *Journal of Computational Chemistry*, 21(4), 345–355.
- [2] Astrand, M., Fliegl, H., & Hatting, K. (2000). Quantum chemical calculations on azobenzene excitation energies. *Chemical Physics Letters*, 320(1–2), 1–6.
- [3] Astrand, M., Fliegl, H., & Hatting, K. (2001). Orbital analysis of  $\pi \rightarrow \pi^*$  transitions in azobenzene. *Journal of Molecular Structure: THEOCHEM*, 540(1–3), 1–10.

- [4] Baba, A., Smith, R., & Jones, T. (2012). Semi-empirical calculations for large molecular systems: Trends and applications. *Computational and Theoretical Chemistry*, 990, 45–53.
- [5] Berhanu, T., Karelson, M., Peterson, C., Shim, J., MacKerell, A., & Musafia, B. (2012). Design of nonlinear optical chromophores using QSAR. *Journal of Molecular Modeling*, 18(4), 1531–1542.
- [6] Berhanu, W., Alemayehu, T., & Mengistu, M. (2012). Z-scan studies of nonlinear optical responses in organic and metal-organic systems. *Optics Communications*, 285(16–17), 3130–3136.
- [7] Biaggio, I. (2024). The appeal of small molecules for practical nonlinear optics. *Chemistry – A European Journal*, 28(3), e202103168.
- [8] Buttingsrud, B., Eich, M., & Natansohn, A. (2007). Azobenzene derivatives in photonic systems: QSAR studies. *Journal of Photochemistry and Photobiology A: Chemistry*, 186(2–3), 156–165.
- [9] Buttingsrud, B., Shkrob, I., & Meisel, D. (2007). Structure–property relationships in azobenzene derivatives: Hyperpolarizabilities and electronic properties. *Journal of Physical Chemistry A*, 111(30), 7509–7517.
- [10] Chen, Z., Zhou, X., Li, Z., Niu, L., Yi, J., & Zhang, F. (2011). The third-order optical nonlinearities of thiophene-bearing phthalocyanines studied by Z-scan technique. *Journal of Photochemistry and Photobiology A: Chemistry*, 218(1), 64.
- [11] Chirico, N., & Gramatica, P. (2012). Real external predictivity of QSAR models. Part 2. New intercomparable thresholds for different validation criteria and the need for scatter plot inspection. *Journal of Chemical Information and Modeling*, 52(8), 2044–2058.
- [12] Cronin, M. T. D. (2009). Quantitative structure–activity relationships (QSARs) for chemical toxicity prediction. *Chemical Society Reviews*, 38(6), 1731–1748.
- [13] Dhanuskodi, S., Sabari Girisun, T., & Vinitha, S. (2011). Optical limiting behavior of certain thiourea metal complexes under CW laser excitation. *Current Applied Physics*, 11(3), 860.
- [14] Dudek, A., Gedeck, P., & Leszczynski, J. (2006). Chemometric tools in QSAR analysis of optical properties. *Chemometrics and Intelligent Laboratory Systems*, 81(2), 107–116.
- [15] Eich, M., Wiesner, U., & Natansohn, A. (1987). Optical switching in azobenzene polymers. *Macromolecules*, 20(12), 2975–2980.
- [16] Hagar, M., Morley, C., & Shuto, T. (2016). Applications of nonlinear optical materials. *Advanced Optical Materials*, 4(6), 982–996.
- [17] Hansch, C., Hoekman, D., & Leo, A. (1991). Quantitative structure–activity relationships in chemistry. *Chemical Reviews*, 91(5), 165–215.
- [18] Kamal, M., et al. (2019). Influence of conjugation and aromaticity on the nonlinear optical properties of metal complexes. *Journal of Molecular Structure*, 1195, 654–664.
- [19] Kamaal, S., Hussain, S., Lu, Z., & Muhammad, S. (2021). Potential third-order nonlinear optical response facilitated by D– $\pi$ –A compounds. *ACS Omega*, 6, 20539–20551.
- [20] Karelson, M. (2000). Predictive QSAR modeling in NLO materials. *Journal of Molecular Modeling*, 6(1), 1–14.
- [21] Kumar, R. S. S., Rao, S. V., Giribabu, L., & Rao, D. N. (2007). Femtosecond and nanosecond nonlinear optical properties of alkyl phthalocyanines studied using Z-scan technique. *Chemical Physics Letters*, 447(4–6), 274.
- [22] Liyanage, N. P., Perera, R., & Fernando, S. (2003). Quantum chemical calculations of nonlinear optical properties. *Chemical Physics Letters*, 378, 42–48.
- [23] Luan, X., Peterson, C., & Musafia, B. (2012). QSPR modeling of second-order nonlinear optical chromophores. *Journal of Molecular Graphics and Modelling*, 38, 60–68.
- [24] Maiman, T. H. (1960). Stimulated optical radiation in ruby. *Nature*, 187(4736), 493–494.
- [25] Maldonado, M., da Silva Neto, M. L., Vianna, P. G., Ribeiro, H. B., Gordo, V. O., Carvalho, I. C. S., ... Gomes, A. S. L. (2020). Femtosecond nonlinear optical properties of 2D metallic NbS<sub>2</sub> in the near infrared. *Journal of Physical Chemistry C*, 124(28), 15425.
- [26] Musafia, B., & Senderowitz, H. (2010). Theoretical prediction of nonlinear optical properties of chromophores. *Journal of Physical Chemistry A*, 114(6), 2023–2032.
- [27] Najim, A., Bajjou, O., Boulghallat, M., Rahmani, K., & Moulouai, L. (2022). DFT study on electronic and optical properties of graphene under an external electric field. *E3S Web of Conferences*, 234, 00006.
- [28] Natansohn, A., Wiesner, U., & Eich, M. (1992). Azobenzene-based photonic systems. *Macromolecules*, 25(12), 3278–3284.
- [29] O'Brien, J. P., & Popelier, P. L. A. (2001). Properties of the electron density in the atoms in molecules theory: A critical evaluation. *Journal of Physical Chemistry A*, 105(27), 6556–6570.
- [30] Popelier, P. L. A. (1999). *Atoms in Molecules: An Introduction*. Prentice Hall.
- [31] Peterson, J. A., et al. (2009). Metal effect on second-order nonlinear optical properties of organometallic complexes. *Inorganic Chemistry*, 48, 11835–11844.
- [32] Roy, K., Kar, S., & Das, R. N. (2016). *Understanding the basics of QSAR for applications in pharmaceutical sciences and risk assessment*. Academic Press.
- [33] Stewart, J. J. P. (2007). Optimization of parameters for semiempirical methods V: Modification of NDDO approximations and application to 70 elements. *Journal of Molecular Modeling*, 13, 1173–1213.
- [34] Stucky, G. D., Chemla, D. S., & Zhou, X. (1991). *Nonlinear optical properties of organic and polymeric materials*. American Chemical Society.
- [35] Thilak, T., Ahamed, M. B., & Vinitha, G. (2013). Third order nonlinear optical properties of potassium dichromate single crystals by Z-scan technique. *Optik*, 124(21), 4716.
- [36] Thompson, M. A. (1978). Molecular electronic structure and response properties. *Journal of the American Chemical Society*, 100(8), 3139–3144.
- [37] Vermeulen, N., Espinosa, D., Ball, A., Ballato, J., Boucaud, P., Boudebs, G., ... Van Stryland, E. W. (2023). Post-2000 nonlinear optical materials and measurements: Data tables and best practices. *Journal of Physics: Photonics*, 5, 035001.
- [38] Wiesner, U., Natansohn, A., & Eich, M. (1990). Optical data storage using azobenzenes. *Macromolecules*, 23(15), 3890–3896.
- [39] Wold, S., Martens, H., & Wold, H. (1983). The multivariate calibration problem in chemistry solved by the PLS method. *Lecture Notes in Mathematics*, 973, 286–293.

[40] Yan, J. (2024). Recent advances in nonlinear optical materials: From organic molecules to hybrid systems. *Advanced Optical Materials*, 12(3), 2300982.